



**HAL**  
open science

## Fatigue crack growth under non-proportional mixed-mode loading in ferritic-pearlitic steel

Véronique Doquet, Sylvie Pommier

► **To cite this version:**

Véronique Doquet, Sylvie Pommier. Fatigue crack growth under non-proportional mixed-mode loading in ferritic-pearlitic steel. *Fatigue and Fracture of Engineering Materials and Structures*, 2004, 27 (11), pp.1051-1060. 10.1111/j.1460-2695.2004.00817.x . hal-01821900

**HAL Id: hal-01821900**

**<https://hal.science/hal-01821900>**

Submitted on 10 Mar 2024

**HAL** is a multi-disciplinary open access archive for the deposit and dissemination of scientific research documents, whether they are published or not. The documents may come from teaching and research institutions in France or abroad, or from public or private research centers.

L'archive ouverte pluridisciplinaire **HAL**, est destinée au dépôt et à la diffusion de documents scientifiques de niveau recherche, publiés ou non, émanant des établissements d'enseignement et de recherche français ou étrangers, des laboratoires publics ou privés.

# Fatigue crack growth under non-proportional mixed-mode loading in ferritic-pearlitic steel

V. DOQUET<sup>1</sup> and S. POMMIER<sup>2</sup>

<sup>1</sup>LMS, Ecole Polytechnique, 91128 Palaiseau, France

<sup>2</sup>LMT, ENS-Cachan, 61, av du Président Wilson, 92235 Cachan, France

Mode II fatigue crack growth tests as well as tests in sequential mode I and then mode II were performed on ferritic-pearlitic steel. For  $K_{II}$  ranging from 7 to 43  $\text{MPa}\sqrt{\text{m}}$ , bifurcation occurs after 12–450  $\mu\text{m}$  of coplanar growth at a decreasing speed. By contrast, hundreds of micrometres of constant speed coplanar growth were obtained under sequential mode I and then mode II loading, for  $\Delta K_{II} = 20\text{MPa}\sqrt{\text{m}}$  and  $\Delta K_I$  ranging from 0.25 to 1.0  $\Delta K_{II}$ . The crack growth rate is a simple sum of the contributions of each mode for  $\Delta K_I = 0.25\Delta K_{II}$  but above this value a synergetic effect is found. The mechanism of this fast-propagation mode is discussed in the light of strain range maps ahead of the crack tip obtained by digital SEM image correlation and elastic-plastic finite element calculations. The stability of the crack path according to the maximum growth rate criterion is demonstrated.

## INTRODUCTION

Surface-initiated cracks in rolling contact fatigue of rails, wheels, bearing or gears are often submitted to a complex sequence of mode I + II loading. Transverse cracks in turbo-generator shafts undergo periodic shear-mode overloads (due to transient torques from electrical faults) superimposed on mode I cyclic loading due to bending. Few studies have been devoted to crack growth under non-proportional mixed-mode loadings and some results suggest that such loadings might be specially damaging.

Nayeb-Hashemi<sup>1</sup> reports marked transient acceleration of mode I crack growth by mode II overloads in AISI 4340 steel (for a distance much lesser than the mode II transient plastic zone size). Reduction in roughness-induced closure due to asperity rubbing during the overload and to the activation of slip planes closer to the crack plane are suggested to explain the transient acceleration. Qian *et al.*<sup>2</sup> report mode I crack growth enhancement by previous cycles in mode II in 2024 aluminium alloy and relate the effect to profuse microcracking that weakens the material around the crack tip. Stanzl *et al.*<sup>3</sup> report an acceleration of mode I crack growth in a 12% chromium steel by a static mode II component for small crack lengths (but above a given length, the mode II component, on the contrary,

is responsible for retardation, for negative  $R$  ratios, because of the induced mismatch between rough fracture surfaces). Wong *et al.*<sup>4,5</sup> applied mode I and II cycles sequentially and observed fast and stable coplanar growth when  $\Delta K_I$  was more than half  $\Delta K_{II}$  in a rail steel, whereas substantial coplanar growth could not be obtained by the combinations of cyclic mode II and static mode I. They proposed empirical equations combining  $\Delta K_I$  and  $\Delta K_{II}$  to correlate kinetic data under sequential loading. The aim of the present study is to improve the understanding of the reasons why such propagation can occur and why it is so fast, through accurate measurements and analysis of crack tip plastic strain and displacement fields during tests performed in a scanning electron microscope (SEM).

## MATERIAL, EXPERIMENTAL AND NUMERICAL PROCEDURES

Steel for railway applications ( $\sigma_{y(0,2)} = 567\text{ MPa}$ ,  $\sigma_u = 898\text{ MPa}$ ) was studied. The microstructure consists of 30  $\mu\text{m}$  wide equiaxial pearlite and ferrite grains. Tubular specimens (10.8 and 9 mm external/internal diameters) with a small hole, 0.5 mm in diameter, as well as 3-mm thick precracked compact tension-shear (CTS) specimens were used (Fig. 1). Precracking was performed in mode I under constant  $\Delta K_I$  ( $7.5\text{ MPa}\sqrt{\text{m}}$ ) and  $R$  (0 until a 1-mm-long crack was formed at the notch tip or on each side

Correspondence: V. Doquet. E-mail: doquet@lms.polytechnique.fr

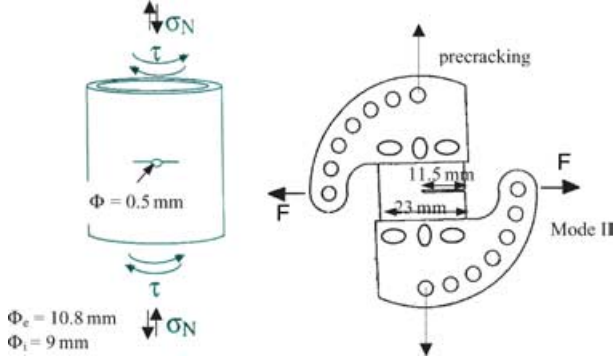


Fig. 1 Geometry of the specimens.

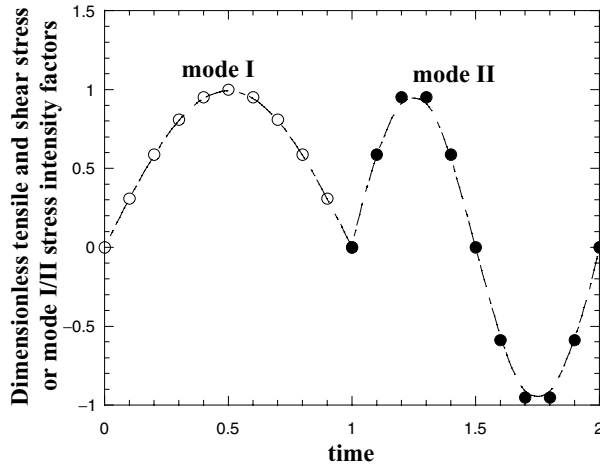


Fig. 2 Loading path used for tests under sequential mode I + II.

of the hole in tubes. Subsequent propagation is thus likely to be affected by residual stresses due to precracking over, at most, one plastic zone size, i.e.  $(1/\alpha\pi) (K_{\max}/\sigma_y)^2 = 55 \mu\text{m}$  at the free surface ( $\alpha = 1$  in plane stress) and  $18 \mu\text{m}$  in the inside ( $\alpha = 1/3$  in plane strain).

Gold microgrids with a  $4\text{-}\mu\text{m}$  pitch were laid ahead of crack tips and along the crack surfaces. Mode II crack propagation tests were carried out at 0.5 Hz with constant nominal  $\Delta K_{II}$  and  $K_{\min}/K_{\max} = 0$  for CTS specimens or  $-1$  for tubular specimens (in the latter case,  $\Delta K_{II}$  is computed as  $2K_{II\max}$  because both parts of the cycle contribute to crack growth). The curvature of the tubes is taken into account in the computation of SIFs using the formulae given by Erdogan & Ratwani.<sup>6</sup> Tests were also performed under sequential mode I ( $R = 0$ ) and then mode II ( $R = -1$ ) loading, at 0.1 Hz, on precracked tubular specimens successively loaded in tension and reversed torsion (Fig. 2).

CTS or tubular specimens were periodically transferred to a tension/torsion loading frame inside an SEM. Crack surface's relative displacements were then measured at both  $K_{\min}$  and  $K_{\max}$  using microgrids as reference marks,

as a function of the distance to the crack tip. Such displacement profiles could be used successfully to derive the effective  $\Delta K_{II}$  and thus take account of crack surface friction, as in a previous study on maraging steel.<sup>7</sup> But due to more extensive crack tip plasticity in the present steel, the exploitation of these data is not straightforward, as explained below.

During sequential mixed-mode tests, correlation of high-resolution digital images of the crack tip area ( $4000 \times 4000$  pixels) taken during a cycle, at  $K_{I\min}$  and  $K_{I\max}$  or  $K_{II\min}$  and  $K_{II\max}$ , respectively, yields the relative displacement field and by differentiation, maps of local strain ranges associated with each loading mode. The precision on the measured displacements is  $\pm 1$  pixel (sub-pixel correlation is possible but has not been attempted here) so that local strains are determined within an error range of  $\pm 0.9\%$ . More details about this technique can be found in Ref. [8].

Finite element analyses have also been conducted using Abaqus in order to distinguish the role of plasticity from that of crack surface friction. A crack in a large rectangular plate with prescribed shear stress along the four sides was modelled (Fig. 3). Quadratic triangular elements and plane stress conditions were employed. The mesh size at crack tip was  $0.25 \mu\text{m}$ . The mesh is adjusted in order to obtain a mean mesh size, over the whole  $K$ -dominance area, of at least one-tenth of the cyclic crack tip plastic zone size. An elastic-plastic constitutive equation with nonlinear kinematic hardening fitted to the experimental stress-strain curves of the material was used. The curvature of tubular specimens and the presence of a hole are not modelled, but the shear stress applied in finite element simulations is calculated so as to obtain the same SIFs as in the tests. The computed displacement profiles in the  $K$ -dominance zone close to the crack tip should be representative of experimental displacements.

## RESULTS

### Mode II

Coplanar crack growth at decreasing rate was observed (Fig. 4a) over a distance increasing from 12 to  $450 \mu\text{m}$  for nominal  $\Delta K_{II}$  ranging from 7.5 to  $43 \text{MPa}\sqrt{\text{m}}$  (Fig. 4b). The mode II kinetic data are plotted in Fig. 4c as a function of the SIFs (effective values when it could be determined as explained below).

For  $\Delta K_{II} = 7.5 \text{MPa}\sqrt{\text{m}}$  and  $R = -1$ , the measured crack surface's relative displacements are well below the theoretical elastic asymptotic profile in plane stress:

$$\Delta u_x = \frac{8\Delta K_{II}^{\text{no min al}}}{E} \sqrt{\frac{r}{2\pi}} \quad (1)$$

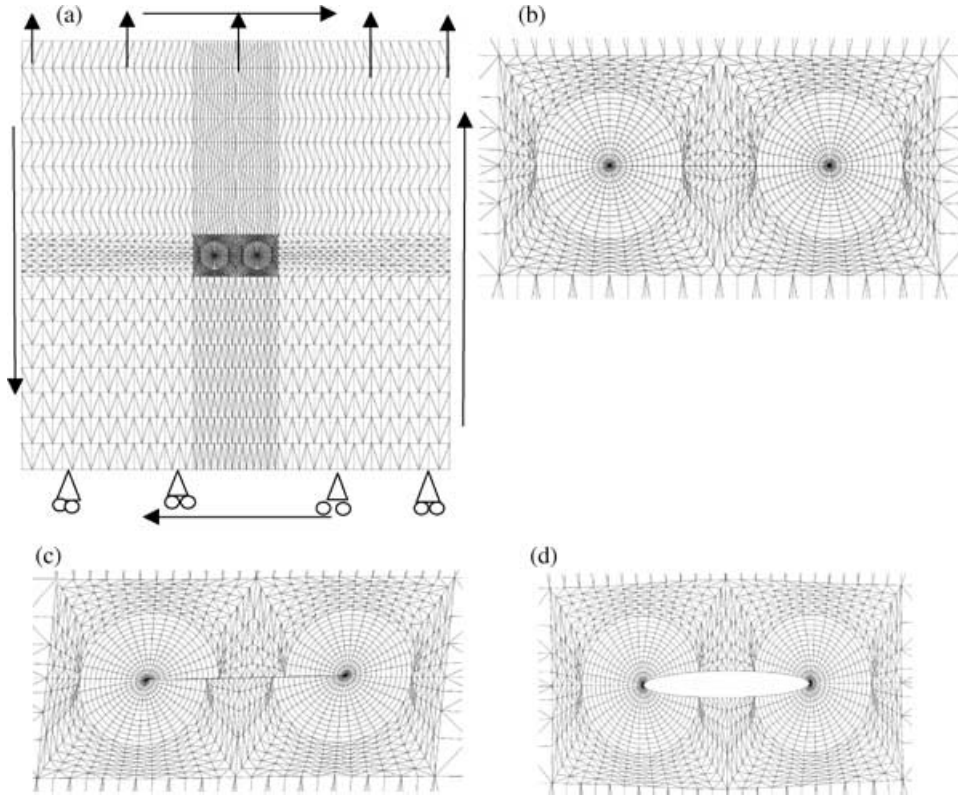


Fig. 3 (a) Finite element mesh and boundary conditions, (b) detail. (c) Deformed mesh in mode II and (d) deformed mesh in mode I.

(Fig. 5a), but are well described by Eq. (1) with an effective  $\Delta K_{II}$  of  $3.5 \text{ MPa}\sqrt{m}$ . Shielding by friction is thus rather important for this loading range.

For  $13.7 \text{ MPa}\sqrt{m}$  (Fig. 5b) and  $R = -1$ , the measured displacements are between the asymptotic elastic sliding displacements and the elastic-plastic values computed by finite elements, over the first  $250 \mu\text{m}$ . For  $43 \text{ MPa}\sqrt{m}$  and  $R = -1$ , the experimental points superpose onto the theoretical elastic asymptotic profile but are well below the elastic-plastic profile.  $\Delta K_{II}^{\text{effective}}$  were thus less than  $13.7 \text{ MPa}\sqrt{m}$  and  $43 \text{ MPa}\sqrt{m}$ , respectively, but it is difficult to specify their values because plasticity can partly compensate the influence of friction on the sliding displacements and lead to overestimated  $\Delta K_{II}^{\text{effective}}$  values (whence the arrows in Fig. 4c).

For  $\Delta K_{II} = 29$  and  $37 \text{ MPa}\sqrt{m}$  and  $R = 0$  (for which  $K_{II\text{max}}$  were higher than for  $R = -1$ , but maximum gross section shear stresses were less than 38% of the 0.2% shear yield stress), measured displacement profiles were above those predicted by linear elastic fracture mechanics (Fig. 6a) but anyway below the ‘elastic-plastic’ profile. The difference between measured and computed elastic-plastic profiles—which can be attributed to friction on the crack surfaces—decreases when crack tip plasticity becomes important and when sliding displacements become

larger than the wavelength of asperities, which is consistent with the literature.<sup>9,10</sup>

It was noticed that for  $R = 0$ , wear of the asperities was faster than during reversed loading, as suggested by the higher flow of debris exuding from the crack surfaces.

An important residual shift of the microgrids at zero load was noticed after a few cycles (Fig. 7). This net shift is partly due to the first loading ramp to  $K_{II\text{max}}$  and partly to ratchetting in the crack surfaces sliding displacement, as evidenced by the 6% increase in microgrids shift measured in an interval of 250 cycles during which crack propagation ( $50 \mu\text{m}$ ) was too small to explain it. This effect was confirmed by FE simulations, as shown in Fig. 6b in which the difference ( $\rho_{II}$ ) between the elastic and the elasto-plastic sliding displacement is plotted. For a given value of  $\Delta K_{II}$ , cyclic plasticity is similar at  $R = -1$  and at  $R = 0$ , though a mean displacement, progressively increased by ratchetting, appears at  $R = 0$  and not at  $R = -1$ . The absence in the experimental results of a clear influence of the  $R$  ratio on the crack growth rates (within the limited data yet available) may thus seem surprising. The material just ahead of the crack tip is probably submitted to non-zero mean shear stress and strain under repeated loading. However, mean stress/strain effects on fatigue lives are known to be much lesser in shear than in push-pull<sup>11,12</sup> and this could

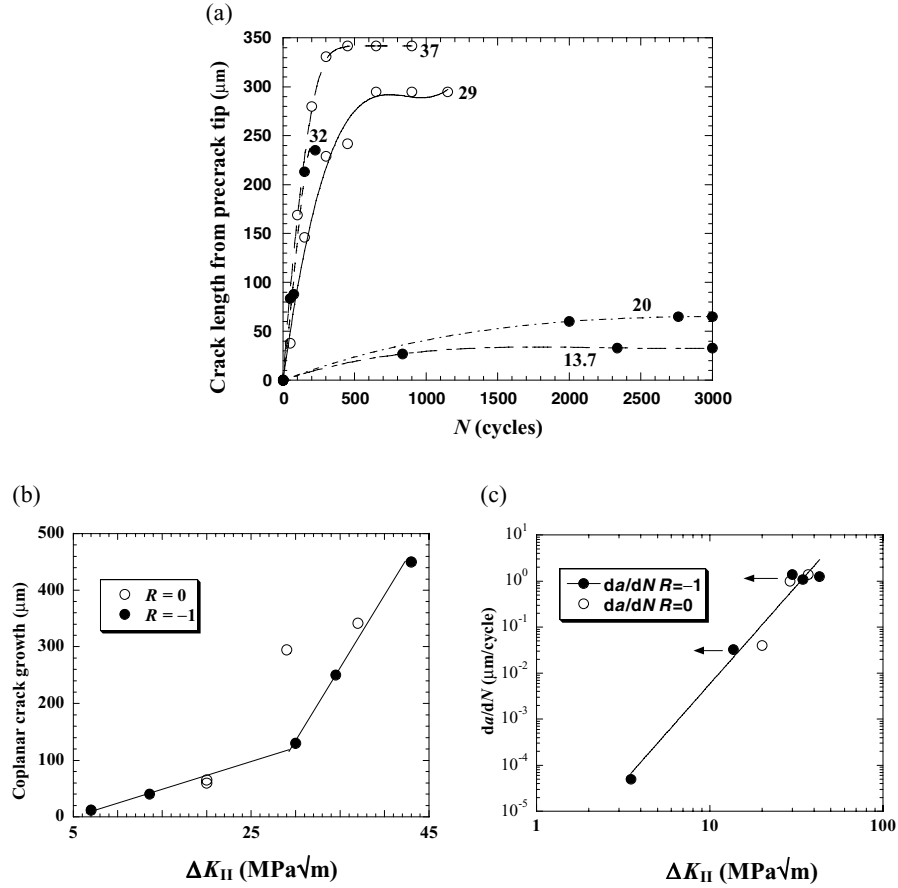


Fig. 4 Synthesis of mode II data. (a) Evolution of crack lengths (the figures refer to applied  $\Delta K_{II}$  in  $\text{MPa}\sqrt{\text{m}}$ ) (b) distance covered in mode II. (c) Crack growth kinetics.

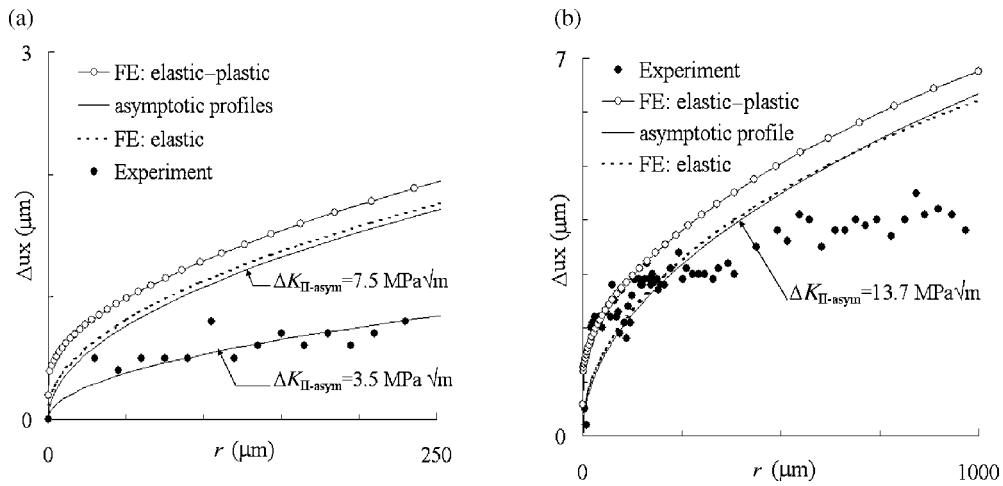
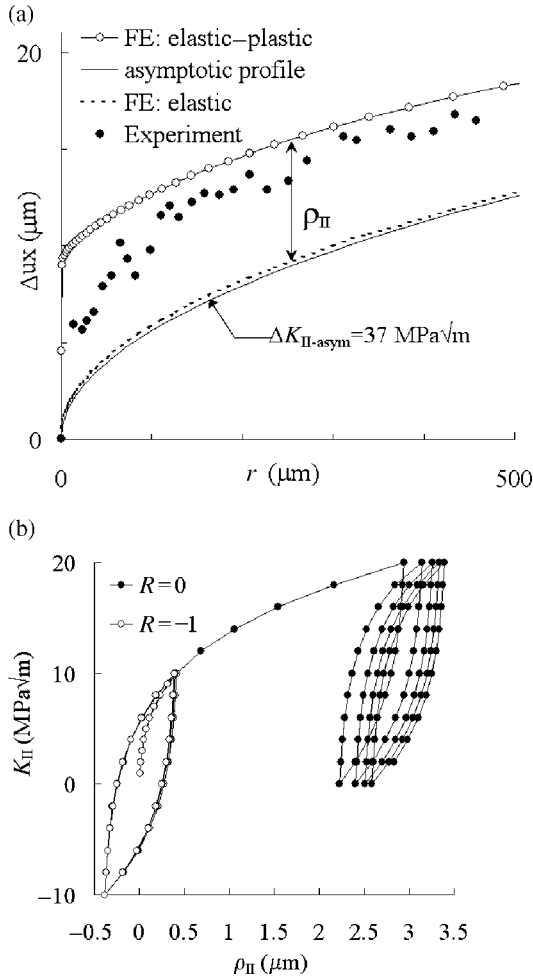


Fig. 5 (a) Sliding displacement profiles for  $R = -1$  with (a)  $\Delta K_{II} = 7.5 \text{ MPa}\sqrt{\text{m}}$  and (b)  $13.7 \text{ MPa}\sqrt{\text{m}}$ .

be the reason for the apparent absence of  $R$  sensitivity of mode II crack growth rates.

Figure 7d shows multiple microcracks, inclined  $70^\circ$  to  $110^\circ$  along the surfaces of the main crack. Such

branches, initiated from secondary slip systems ( $\tau_{r\theta}$  has a secondary maximum in this angular range), have been shown to shield the main crack tip<sup>13</sup> and contribute, in addition to the increasing energy dissipated by friction,



**Fig. 6** (a) Sliding displacement profiles for  $\Delta K_{II} = 37 \text{ MPa}\sqrt{m}$ ,  $R = 0$ . (b) Evolution of the ‘plastic sliding displacement’  $\rho_{II}$  computed  $250 \mu\text{m}$  behind the crack tip for  $\Delta K_{II} = 20 \text{ MPa}\sqrt{m}$ .

to the deceleration and final bifurcation of mode II cracks.

### Sequential mode I-II

Figure 8a shows the evolution of the half crack length measured during two tests under sequential mode I + II with  $\Delta K_{II} = 20 \text{ MPa}\sqrt{m}$ . For the first test,  $\Delta K_I$  was initially equal to  $\Delta K_{II}$ , later reduced to  $0.75\Delta K_{II}$ ,  $0.5\Delta K_{II}$ ,  $0.25\Delta K_{II}$ , and finally to zero (the latter condition leading to immediate bifurcation). For the second test,  $\Delta K_I$  was  $0.35\Delta K_{II}$ . No deceleration appears when the crack propagates over several hundreds of micrometres, under constant nominal  $\Delta K_{II}$  (whereas bifurcation occurs after only  $65 \mu\text{m}$  coplanar growth for the same  $\Delta K_{II}$  in mode II) and compared to what is observed in pure mode II, the quan-

tity of fretting debris ejected by the surfaces is limited, which suggests an attenuation of friction forces.

Fractographic observations on the second specimen ( $\Delta K_I = 0.35\Delta K_{II}$ ) confirm this point (Fig. 9); even though signs of rubbing can be observed here and there, fracture surfaces are not completely mated by friction as it is in pure mode II. Note the absence of mode I striations as also reported by Wong *et al.*<sup>5</sup>

The aspect of fracture surfaces cannot be explained by the intermittent opening due to mode I cycles because it should not prevent crack surface’s friction during the mode II part of the cycle. Finite element simulations are helpful to explain this observation. Figure 10a compares the evolution of the ‘plastic part of sliding and opening displacements’ computed  $250 \mu\text{m}$  behind the crack tip during pure mode I, pure mode II and sequential mode I + II, during the second, third and fifth cycles for  $\Delta K_I = 0.75\Delta K_{II}$  (note that the loading sequence applied in the simulations is one cycle in mode II followed by one cycle in mode I contrary to Fig. 2). The opening does not fall to zero during the mode II part of the cycle and ratchetting in the crack opening clearly appears. Even though the minimum opening computed over the fifth cycle,  $0.08 \mu\text{m}$ , is lesser compared to the height of the asperities of the crack surfaces—a few micrometres—the increase in  $\rho_I$  due to ratchetting seems fast enough that in a few hundred cycles the separation between the crack surfaces overcomes the height of a majority of these asperities. This could explain the strong attenuation of crack surface’s friction. A slight ratchetting towards negative shear displacements also appears.

As there is no deceleration, a unique growth rate can be defined for each mode-mixity ratio. Figure 8b shows the evolution of the growth rate with  $\Delta K_I$ . Open symbols correspond to a simple sum of the mode I and mode II growth rates for the corresponding SIFs. The measured growth rates are clearly higher than these estimates (a factor of three higher when  $\Delta K_I$  reaches  $\Delta K_{II}$ ), which means that a synergetic effect is present in agreement with the results of Wong *et al.*<sup>4,5</sup> for a rail steel.

The evolution of the ‘plastic part of the opening displacement’,  $\rho_I$ , computed during pure mode I or sequential mode I + II loading is plotted in Fig. 10b versus the applied mode I stress intensity factor. It is observed that the amplitude of variation of  $\rho_I$  is almost four times higher in sequential mode I-II than in pure mode I. This effect can significantly contribute to the observed synergetic effect of mode I and mode II found in the experiments (Fig. 8b). A fatigue crack growth rate higher in sequential I-II than in pure mode I can be inherited from a higher amplitude of crack tip opening displacement in sequential I-II than in pure mode I.

As concerns the aspect of the crack developed during the first test, the roughness as well as the number and the

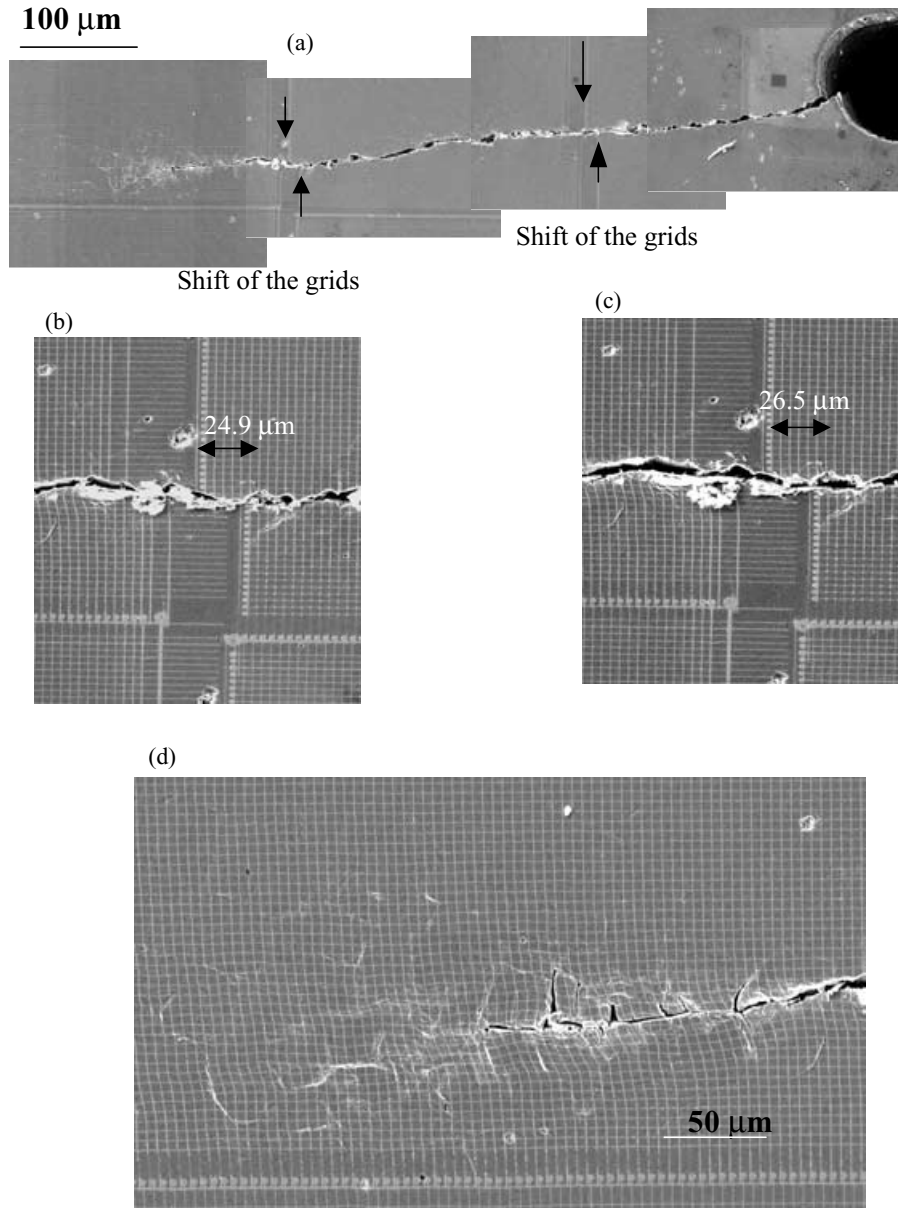


**Fig. 7** Aspect of a crack at zero load for  $\Delta K_{II} = 37 \text{ MPa}\sqrt{m}$  and  $R = 0$  (a) whole length after 200 cycles, (b) detail after 200 cycles, (c) same detail after 450 cycles, (d) microcracks initiated along secondary slip systems shielding the main crack tip.

length of aborted branches increase as  $\Delta K_I$  decreases, but the average direction of propagation, however, remains unchanged (Fig. 11a). Figure 11b shows the aspect of the crack developed in the second specimen, with  $\Delta K_{II} = 20 \text{ MPa}\sqrt{m}$  and  $\Delta K_I = 0.35 \Delta K_{II}$ , which is rather straight at a microscale.

Figures 12a and b show the shear and tensile strain range profiles measured ahead of the crack tip by digital image correlation during the mode II stage of the cycle for  $\Delta K_I = \Delta K_{II}$ . It can be observed that large tensile plastic strains are produced by the mode II cycle along a line theoretically loaded in pure shear. Conversely (Figs 9c and

d), large shear strains are measured along the ligament during the mode I part of a cycle.

This coupling is less pronounced when  $\Delta K_I = 0.75 \Delta K_{II}$ . That is why it is not suspected to be due to some asperity-induced opening of the crack, which has no reason to decrease in those cases where, on the contrary, roughness increases. Furthermore, the plastic flow in shear measured along the ligament during the tensile part of the cycle cannot be attributed to some mode II component because the corresponding images of the crack surfaces do not suggest any sliding displacement. Strain measurements along the ligament were performed on CTS specimens loaded in

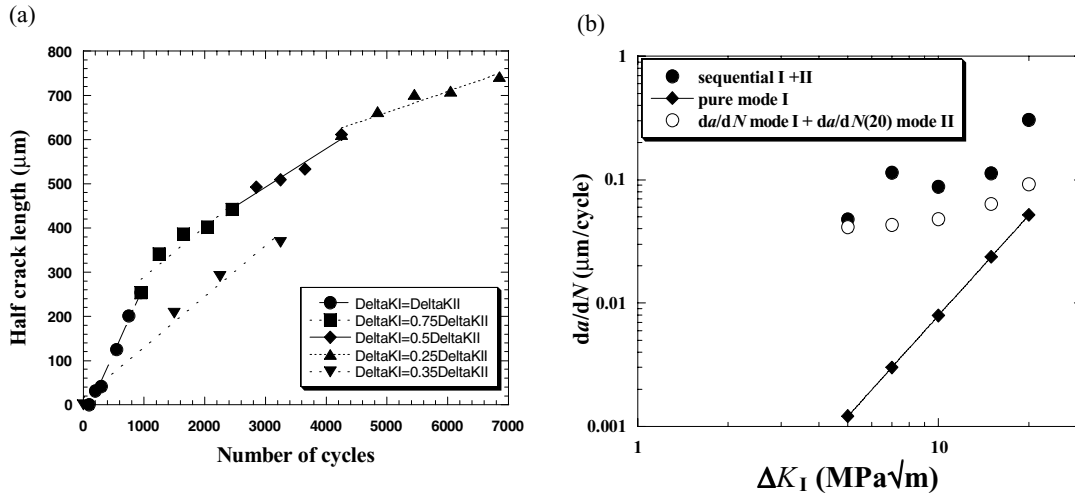


Fig. 8 Kinetic data for sequential mode I-II.

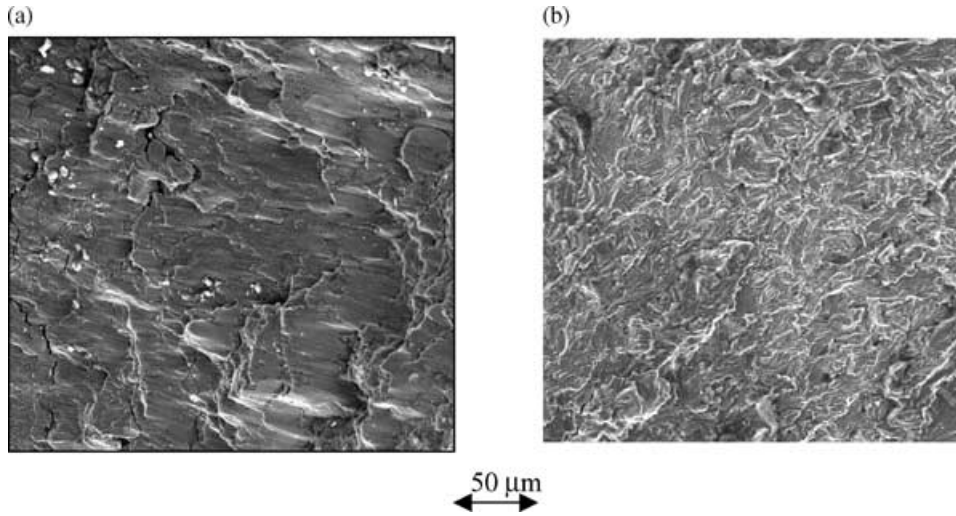


Fig. 9 Fracture surfaces (a) mode II,  $\Delta K_{II} = 13.7 \text{ MPa}\sqrt{m}$ ,  $R = -1$  (b) sequential mode I + II,  $\Delta K_I = 7 \text{ MPa}\sqrt{m}$ ,  $\Delta K_{II} = 20 \text{ MPa}\sqrt{m}$ .

pure mode II for comparison. It did not reveal any significant tensile plastic flow.

## DISCUSSION

The stability of coplanar growth down to a mode-mixity ratio of 0.25 observed in the present study contrasts with the results of Wong *et al.*<sup>4,5</sup> who observed bifurcations when  $\Delta K_I$  dropped below  $0.5\Delta K_{II}$ . However, note that Wong *et al.* applied equibiaxial tension during the mode I part of the cycles, which means that a tensile non-singular T stress, parallel to the crack was present. Such a stress has been shown, through analytical and numerical calculations, by Cotterell & Rice<sup>14</sup> or by Frelat & Leblond<sup>15</sup> to be favourable to crack deviation. Torsional fatigue tests with superimposed static tensile stress performed by Zhang &

Akid<sup>16</sup> on 316L stainless steel also led to earlier bifurcations from Stage I to Stage II than in pure torsion.

Residual stresses left just ahead of the crack by the mode I cycle might explain the observation of Fig. 12, as illustrated by Fig. 13a, which shows a schematic two-dimensional section of the elastic domain of the material translated by kinematic hardening during the mode I plastic flow. During the subsequent cycle in mode II, plastic flow will thus be easier (the vertical cord is smaller than the diameter) and, due to the normality of plastic flow, both tensile and shear plastic strains will be produced, instead of pure shear for an annealed metal. In addition, ratchetting will lead to the accumulation of tensile strain because the sign of the axial strain produced by reversed shear loading will be the same as in the forward sense. (Note that this drawing is somewhat simplified because

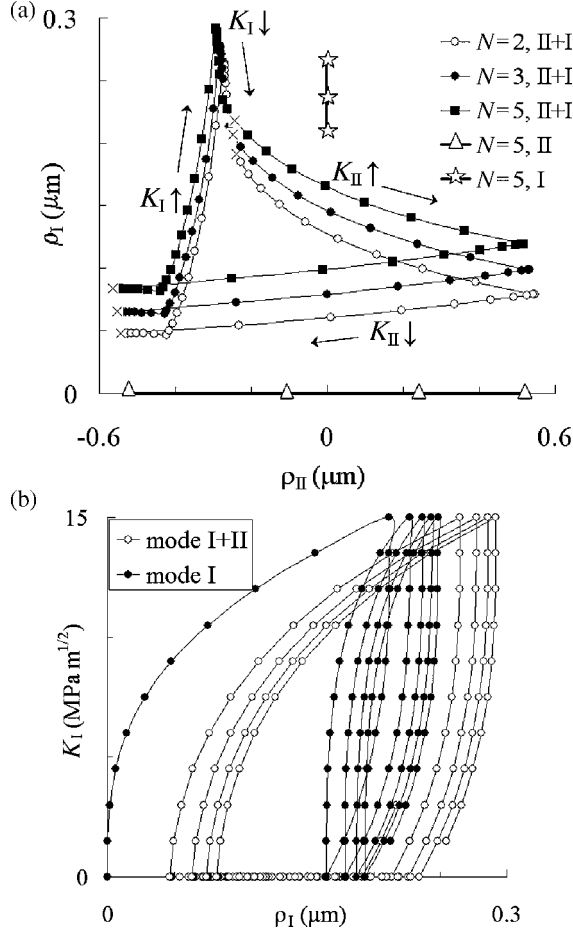


**Fig. 10** Evolution of the ‘plastic sliding and opening displacements’ computed  $250 \mu\text{m}$  behind the crack tip in pure mode I, pure mode II or sequential mode I + II,  $\Delta K_I = 0.75 \Delta K_{II}$  (a)  $\rho_I$  versus  $\rho_{II}$ . (b)  $K_I$  versus  $\rho_I$ .

the shift of the elastic domain associated with plastic flow at points A and B (which should slightly relax the residual compressive stress) has not been represented.)

A symmetrical mechanism (Fig. 13b) could lead to the accumulation of shear strain during the mode I stage of the cycles. If, thanks to intermittent mode I,  $\Delta K_{II}^{\text{effective}}$  stays constant and almost equal to  $\Delta K_{II}^{\text{nominal}} = 20 \text{ MPa}\sqrt{\text{m}}$  instead of decreasing with crack length, as in pure mode II, this would explain the stability of the crack path for  $\Delta K_I = 0.25 \Delta K_{II}$ , a case for which synergetic effects due to plasticity are not observed in terms of growth rate. Knowing  $K_I(t)$ ,  $K_{II}(t)$  for the main crack, and using the functions tabulated by Amestoy *et al.*,<sup>17</sup> the SIFs on any potential infinitesimal branch crack in the direction  $\theta$ ,  $k_1^*(t, \theta)$ ,  $k_2^*(t, \theta)$  can be computed as:

$$\begin{pmatrix} k_1^*(t) \\ k_2^*(t) \end{pmatrix} = \begin{pmatrix} F_{11}(\theta) & F_{12}(\theta) \\ F_{21}(\theta) & F_{22}(\theta) \end{pmatrix} \begin{pmatrix} K_I(t) \\ K_{II}(t) \end{pmatrix} \quad (2)$$

and their range over one cycle  $\Delta k_1^*(\theta)$ ,  $\Delta k_2^*(\theta)$  deduced.

For the first part of the sequential test ( $\Delta K_I = \Delta K_{II}$ , Fig. 14a)  $\Delta k_1^*$  and  $\Delta k_2^*$  are both maximum for  $\theta \approx 0^\circ$  and no facet satisfies the ‘local symmetry’ criterion ( $\Delta k_2^* = 0$ ) so that coplanar growth is necessarily stable. For the fourth part of the sequential test ( $\Delta K_I = 0.25 \Delta K_{II}$ , Fig. 14b)  $\Delta k_1^*$  is maximum ( $12.3 \text{ MPa}\sqrt{\text{m}}$ ) and  $\Delta k_2^*$  minimum ( $2.2 \text{ MPa}\sqrt{\text{m}}$ ) for  $\theta \approx 75^\circ$ . The growth rate along this potential direction, computed from the mode I data provided by Ascometal (the mode II contribution is negligible), appears to be 3.4 times lesser than the coplanar growth rate during sequential mixed-mode loading. According to the maximum growth-rate criterion first proposed by Hourlier & Pineau,<sup>18</sup> coplanar growth should thus be preferred.

## CONCLUSIONS AND FINAL REMARKS

For a given  $\Delta K_{II}$ , wear of asperities, ratchetting and plasticity at the crack tip are more important for  $R = 0$  than for  $R = -1$ . This was shown by microgrid’s distortions as well as FE simulations. Similar crack growth rates seem, however, to result for a given nominal  $\Delta K_{II}$ . Under sequential mixed mode loading, coplanar growth seems stable (less friction, no deceleration) down to a mode-mixity ratio of 0.25.

For small  $\Delta K_I$ , the role of mode I cycles seems mainly to periodically unlock crack surfaces and to keep the effective  $\Delta K_{II}$  constant. The contributions of each mode to the growth rate are simply added.

For higher  $\Delta K_I$ , in addition to the periodic release of friction forces, a synergetic effect (partly due to a strong increase in the amplitude of plastic crack opening  $\Delta \rho_I$  and partly to residual stresses and normality of plastic flow giving rise to biaxial ratchetting) accelerates the crack growth.

The maximum growth-rate criterion rationalizes the crack path observed in such non-proportional loadings. However, further research is needed to investigate the influence of the loading path. Are effective SIFs or empirical combinations of effective SIFs sufficient to describe crack growth rates under non-proportional loadings? Such parameters capture the influence of mode II on closure effects and mode I on friction effects but not the complex interactions in terms of crack tip plastic flow that are likely to be quite loading path-dependent and to vary substantially with the material behaviour (kinematic or isotropic hardening, degree of additional hardening under non-proportional loading). A recent numerical analysis of Wong’s results by Dahlin & Olsson<sup>19</sup> also led the authors to the conclusion that plasticity effects have to be captured to predict crack growth rates under non-proportional loading.

## Acknowledgements

This study was partly supported by Ascometal-CREAS.

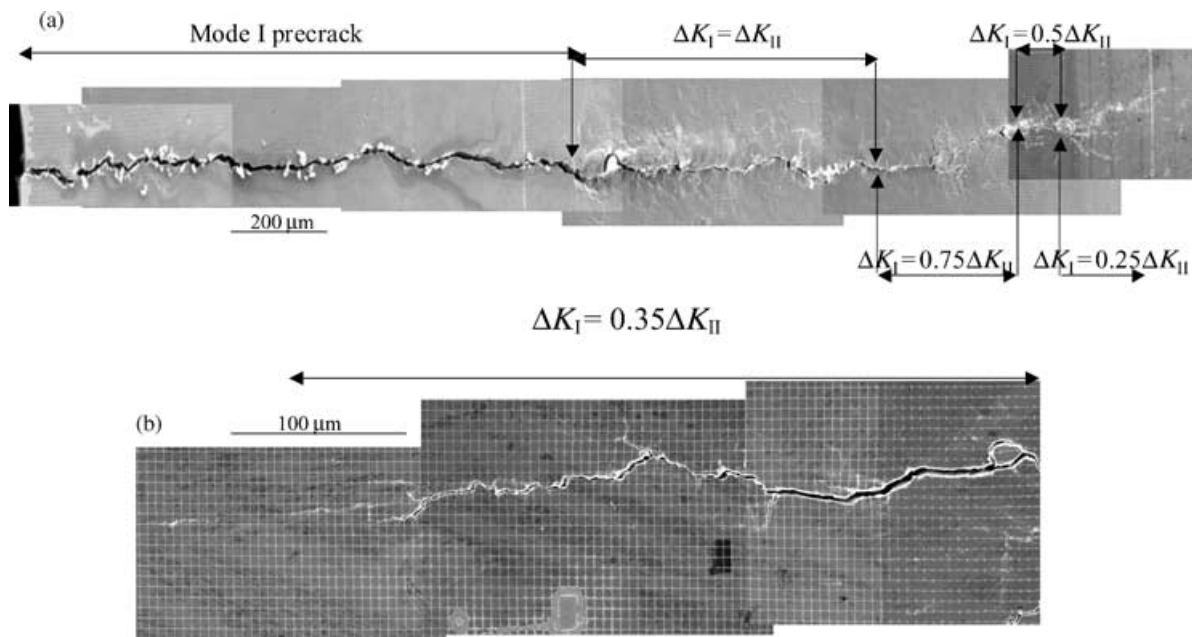


Fig. 11 Aspect of cracks developed in sequential mode I + II.

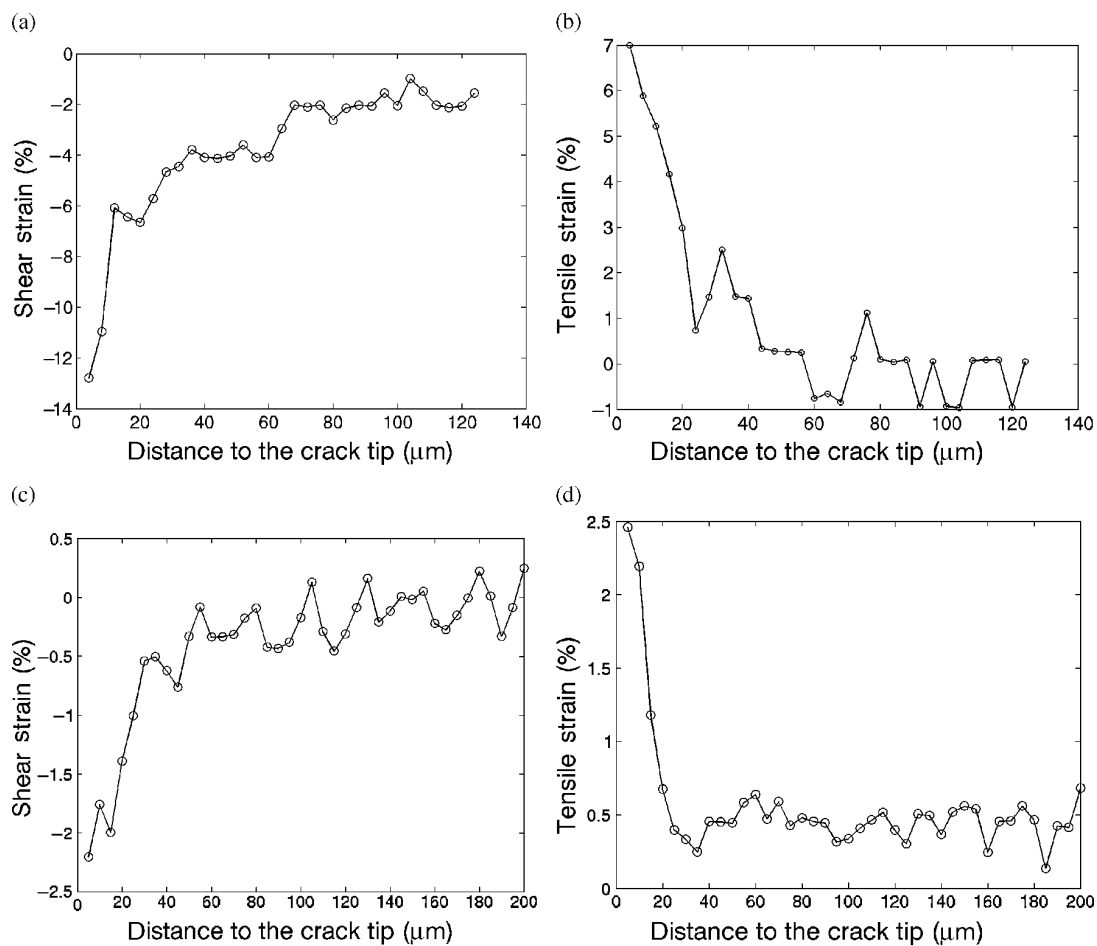
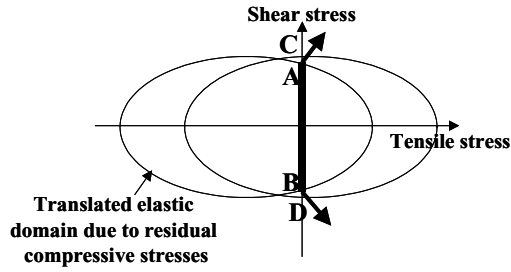


Fig. 12 (a) Shear and (b) tensile strain range profiles measured along the ligament during the mode II stage of the sequential cycle,  $\Delta K_I = \Delta K_{II}$  (c) and (d) same for the mode I part of the cycle.

(a) Mode II cycle



(b) Mode I cycle

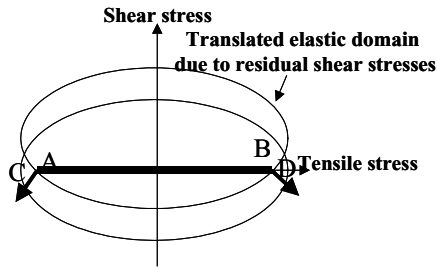


Fig. 13 Schematic of plastic flow during the mode II or mode I part of a sequential test.

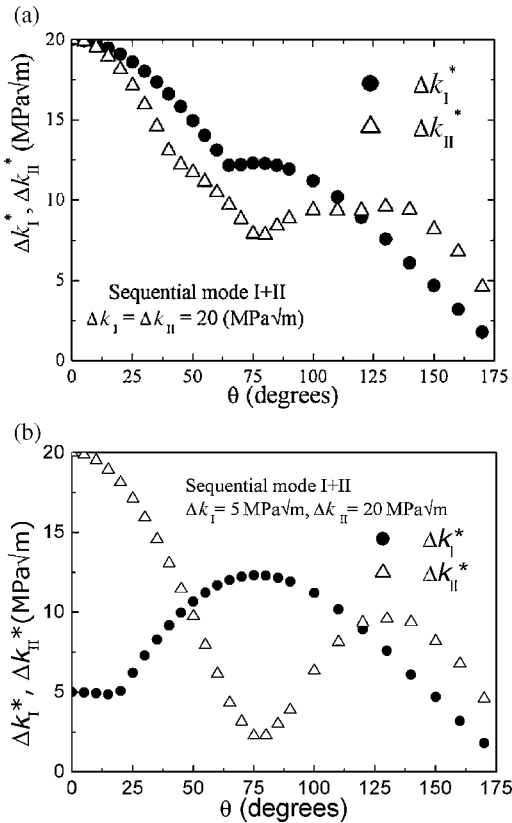


Fig. 14 Mode I and mode II SIFs on an infinitesimal branch crack as a function of its orientation for (a)  $\Delta k_I = \Delta k_{II}$  and (b)  $\Delta k_I = 0.25\Delta k_{II}$ .

REFERENCES

- Nayeb-Hashemi, H. (1989) Effects of mode I and mode II overloads on subsequent mode I crack growth in AISI 4340 steels. *Biaxial and Multiaxial Fatigue, EGF3* (Edited by M. W. Brown & K. J. Miller), MEP, London, pp. 265–283.
- Qian, C. F., Charles, P. R. and Li, J. C. M. (1997) Effect of mode II loading on mode I fatigue crack growth. *Engng Fract. Mech.* **56**, 593–602.
- Stanzl, S. E., Czegley, M., Mayer, H. R. and Tschegg, E. (1989) Fatigue crack growth under combined Mode I and Mode II loading. *Fracture Mechanics: Perspectives and Directions (Twentieth Symposium)*. ASTM STP 1020 (Edited by R. P. Wei & R. P. Gangloff), Philadelphia PA, pp. 479–496.
- Wong, S. L., Bold, P. E., Brown, M. W. and Allen, R. J. (1996) A branch criterion for shallow angled rolling contact fatigue cracks in rails. *Wear* **191**, 45–53.
- Wong, S. L., Bold, P. E., Brown, M. W. and Allen, R. J. (2000) Fatigue crack growth rates under sequential mixed-mode I and II loading cycles. *Fatigue Fract. Engng Mater. Struct.* **23**, 667–674.
- Erdogan, F. and Ratwani, M. (1972) A circumferential crack in a cylindrical shell under torsion. *Int. J. Fract. Mech.* **8-1**, 87–95.
- Pinna, C. and Doquet, V. (1999) The preferred fatigue crack propagation mode in a M250 maraging steel loaded in shear. *Fatigue Fract. Engng Mater. Struct.* **22**, 173–183.
- Allais, L., Bornert, M., Bretheau, T. and Caldemaison, D. (1994) Experimental characterization of the local strain field in a heterogeneous elastoplastic material. *Acta Met. Mater.* **42**, 3865–3880.
- Tschegg, E. K. (1983) Sliding mode crack closure and mode III fatigue crack growth in mild steel. *Acta Met.* **31-9**, 1323–1330.
- Gross, T. S. and Mendelsohn, D. A. (1988) On the effect of crack face contact and friction due to fracture surface roughness in edge cracks subjected to external shear. *Engng Fract. Mech.* **31-33**, 405–420.
- Hurd, N. J. and Irving, P. E. (1985) Smooth specimen fatigue lives and microcrack growth modes in torsion. *Multiaxial Fatigue*. ASTM STP 853 (Edited by K. J. Miller & M. W. Brown). ASTM, Philadelphia, PA, pp. 267–284.
- Fatemi, A. and Kurath, P. (1988) Multiaxial fatigue life predictions under the influence of mean stresses. *J. Engng Mater. Tech.* **110**, 380–388.
- Doquet, V. and Frelat, J. (2001) Branch crack development from the surface of a fatigue crack propagating in mode II. *Fatigue Fract. Engng Mater. Struct.* **24**, 207–214.
- Cotterell, B. and Rice, J. R. (1980) Slightly curved or kinked cracks. *Int. J. Fract* **16**, 155–169.
- Frelat, J. and Leblond, J. B. (1999) Crack branching from an initially closed crack in the presence of friction. *Comptes Rendus Acad. Sci. Paris t.327, Série II b*, 1251–1258.
- Zhang, W. and Akid, R. (1997) Mechanisms and fatigue performance of two steels in cyclic torsion with axial static tension/compression. *Fatigue Fract. Engng Mater. Struct.* **20**, 547–557.
- Amestoy, M., Bui, H. D. and Dang Van, K. (1979) Déviation infinitésimale d'une fissure dans une direction arbitraire. *Comptes Rendus Acad. Sci. Paris B289*, 99–102.
- Hourlier, F., d'Hondt, H., Truchon, M. and Pineau, A. (1985) Fatigue crack path behavior under polymodal fatigue. *Multiaxial Fatigue, ASTM STP 853* (Edited by K. J. Miller & M. W. Brown). ASTM, Philadelphia, PA pp. 228–248.
- Dahlin, P. and Olsson, M. (2003) The effect of plasticity on incipient mixed-mode fatigue crack growth. *Fatigue Fract. Engng Mater. Struct.* **26**, 577–588.